





Article

Influence of Heat Treatment Parameters on the Microstructure of 17-4 PH Single Tracks Fabricated by Direct Energy Deposition

Mattia Merlin ¹, Cindy Morales ^{1,*}, Matteo Ferroni ^{2,3}, Annalisa Fortini ¹ and Chiara Soffritti ¹

¹ Department of Engineering (DE), University of Ferrara, Via Saragat 1, 44122 Ferrara, Italy; mrlmmt@unife.it (M.M.); frtnls@unife.it (A.F.); chiara.soffritti@unife.it (C.S.)

² Department of Civil Engineering, Architecture, Land, Environment and of Mathematics (DICATAM), University of Brescia, Via Branze 43, 25123 Brescia, Italy; frmtt@unife.it

³ CNR-IMM, Institute for Microelectronics and Microsystems, Via P. Gobetti 101, 40129 Bologna, Italy

* Correspondence: mrlcdy@unife.it

Abstract: Post-fabrication heat treatment (PFHT) is one of the most applied strategies for achieving the desired microstructure and mechanical resistance on additive manufactured components because of the non-equilibrium microstructural state of the material in the as-built condition. In particular, during PFHT, 17-4 PH martensitic stainless steel is mainly strengthened by the precipitation of Cu-rich nanometric particles and Nb carbides into the metal matrix. In this work, the influence of specifically designed PFHTs on the microstructural and mechanical properties of 17-4 PH single tracks fabricated via direct energy deposition was studied. Different solubilization and aging times, as well as a direct aging strategy, were considered. Optical microscopy, X-ray diffractometry, and transmission electron microscopy were used to investigate the microstructure evolution induced by the PFHTs. Moreover, Vickers microhardness measurements were performed to evaluate the increase in mechanical strength. In all cases, the heat-treated single tracks showed a mean microhardness higher than that of the depositions in the as-built condition. In the single tracks subjected to solution treatment, followed by aging for about 100 h, the presence of both Cu-rich precipitates and Nb carbides was assessed; conversely, when directly aged from the as-built condition, only Nb carbides were detected. In the latter case, the carbides were finer and closer to each other than those in the single tracks aged after the solution treatment.

Keywords: 17-4 PH steel; laser-direct energy deposition; heat treatment; transmission electron microscopy; hardness



Citation: Merlin, M.; Morales, C.; Ferroni, M.; Fortini, A.; Soffritti, C. Influence of Heat Treatment Parameters on the Microstructure of 17-4 PH Single Tracks Fabricated by Direct Energy Deposition. *Appl. Sci.* **2024**, *14*, 700. <https://doi.org/10.3390/app14020700>

Academic Editor: Ana M. Camacho

Received: 15 December 2023

Revised: 5 January 2024

Accepted: 12 January 2024

Published: 14 January 2024



Copyright: © 2024 by the authors. Licensee MDPI, Basel, Switzerland. This article is an open access article distributed under the terms and conditions of the Creative Commons Attribution (CC BY) license (<https://creativecommons.org/licenses/by/4.0/>).

1. Introduction

Martensitic precipitation-hardening stainless steels, such as 17-4 PH, are characterized by a low percentage of carbon and mainly contain chromium and nickel as their major alloying elements [1–3]. The 17-4 PH steel is intensively used in several industrial sectors, such as aeronautics and the automotive industry, for manufacturing components through conventional forming processes and welding. More recently, additive manufacturing (AM) processes [4–6], specifically, laser-direct energy deposition (L-DED) [7–10] and laser-powder bed fusion (L-PBF) [11–15] techniques, have demonstrated several advantages in the fabrication of structural components with 17-4 PH steel. In particular, the L-DED process consists of a laser source that melts a feedstock powder material simultaneously as it is supplied through a nozzle, until the part is built. The high energy density provided by the laser induces an ultra-high cooling rate, considerably impacting the microstructure and the mechanical properties of the deposited part [16]. It is well-known that post-fabrication heat treatments (PFHTs) become crucial to enhance the properties of AM components [17–20]. The strengthening of 17-4 PH steel results from a combination of the martensitic matrix and the precipitation of nanometric particles, mainly Cu-rich precipitates (CRPs) and fine Nb carbides [21]. The precipitation of these particles is usually obtained by the H900

heat treatment, which involves a solution treatment followed by aging at 480 °C [22,23]. In the literature, the H900 heat treatment is the most widely studied, but other post-fabrication heat treatment routes, such as the only solution treatment [19,24–26], solution treatment + aging [26–29], the only aging treatment [26,30–32], and solution treatment + over-aging [27,33], are discussed. In the study performed by Sowa et al. in 2015 [34], the effects of a double solution treatment on the microstructural features and hardness of wrought 17-4 PH steel samples were investigated. Specifically, this treatment consisted of a double solution treatment at 1028 °C for 1 h, followed by aging at 540 °C for 4 h. The heat-treated samples revealed the full presence of lathy martensite with irregular grain growth, indicating the complete transformation of the retained austenite. Unfortunately, the aging parameters promoted a drop in the material hardness due to the long-time aging duration. These results are similar to those reported by Ziewiec et al. in [33]. In this work, welded 17-4 PH steel samples were aged at temperatures between 480 °C and 620 °C and for holding times from 1 h to 4 h. The authors further confirmed a hardness decrease in samples treated at 540 °C and 620 °C due to the over-aging phenomenon. Concerning the precipitation of strengthening particles, it was also emphasized that, at 620 °C, the precipitation of a significant amount of CRP and carbide particles may occur, but these precipitates became coarser when increasing the holding time.

Another study on the influence of aging parameters on the microstructure of a 17-4 PH bar was conducted by Viswanathan et al. [35]. The authors performed a traditional solution treatment at 1040 °C for 30 min, followed by quenching in iced water and subsequent aging at different temperatures (470 °C, 510 °C, and 600 °C) for durations ranging from 5 min to 8 h. The authors noted the presence of CRPs in the microstructure above 470 °C, but when the samples were heat-treated at 510 °C for 2 h, the precipitation of $M_{23}C_6$ arose, enhancing their hardness behavior. Nevertheless, at 510 °C, an increase in the aging time from 2 h to 8 h, as well as an aging treatment carried out at 600 °C for 1 h, resulted in the coarsening of these precipitates, causing a critical hardness drop. In another study, Murayama et al. [36] investigated the effects of long aging times (100 and 5000 h) on the microstructure of 17-4 PH steel samples using transmission electron microscopy. The authors observed the presence of nanometric CRPs after 5000 h of aging, along with Nb-Cr-rich carbides. The formation of both kinds of particles was found to enhance their hardness after the first 100 h of aging at temperatures above 400 °C.

Focusing on the analysis of heat treatment effects on AM parts, Sun et al. [37] compared the microstructural evolution of additively manufactured 17-4 PH parts with that of wrought components, with the aim of evaluating the influence of a traditional H900 post-fabrication heat treatment route. The results showed that the AM and wrought samples were similar in terms of their hardness and the distribution of the microstructural constituents after PFHT. Hsu et al. [26] analyzed the effects of several heat treatment routes on 17-4 PH samples fabricated via selective laser melting (SLM); specific attention was paid to direct aging (without solution treatment), since it was able to guarantee the highest improvement in mechanical properties. Meredith et al. [27] performed an analysis of different heat treatment strategies on powder bed fusion 17-4 PH samples, including, once again, direct aging and the only solution treatment. The authors correlated the efficacy of the heat treatments with the composition of the raw material in terms of the Ni/Cr ratio, and with the fabrication process used for manufacturing the feedstock powder. Finally, AlMangour and Yang [38] investigated the application of direct aging performed at 480 °C and 590 °C to 17-4 PH steel samples fabricated via direct metal laser sintering (DMLS). The authors found that the direct aging was effective in improving the mechanical properties.

To the best of the authors' knowledge, no research in the literature has evaluated the effects of different heat treatment routes on L-DED 17-4 PH single-track samples. In this regard, this paper aims to address this gap by focusing on the influence of tailored PFHTs on L-DED 17-4 PH single tracks deposited on an AISI 316L steel plate. The substrate was selected considering its corrosion resistance, chemical compatibility with 17-4 PH steel, and widespread industrial applications. The microstructure and phase compositions of

the specimens were determined using optical microscopy (OM) and X-ray diffractometry (XRD). As a possible cause of the strengthening of the material, the precipitation of Cu-rich particles and Nb carbides in the matrix was assessed using transmission electron microscopy (TEM). At last, the mechanical properties were investigated using Vickers microhardness measurements.

2. Materials and Methods

Gas-atomized 17-4 PH steel powders, provided by Böhler (Böhler-Uddeholm, Vienna, Austria), whose nominal chemical composition is reported in Table 1, were used to deposit single tracks onto a $120 \times 40 \times 10 \text{ mm}^3$ AISI 316L stainless steel plate. As declared by the supplier, the powders had a near-spherical shape with some rough agglomerated satellites and a few elongated particles, ranging from 45 to 90 μm in diameter. A six-axis ABB IRB 4600 robot (ABB, Zurich, Switzerland), available at the Birex Competence Center (Bologna, Italy) and equipped with a v2.0 CLAMIR camera (CLAMIR, Madrid, Spain), was employed to fabricate the depositions.

Table 1. Nominal chemical composition (wt. %) of the 17-4 PH powders used for the single-track depositions.

Element	Si	Cr	Ni	Cu	Nb	Mn	P	S	C	Fe
Chemical composition (wt. %)	0.43	15.28	4.49	3.39	0.27	0.50	0.019	0.0003	0.039	Balance

The optimal process parameters were chosen according to a preliminary investigation by the same authors [8]. Figure 1 depicts a scheme of the fabricated depositions, which consists of three 100 mm long single-track replicas (denoted as A, B, and C in Figure 1) being deposited with the selected process parameters on the AISI 316L substrate [8].

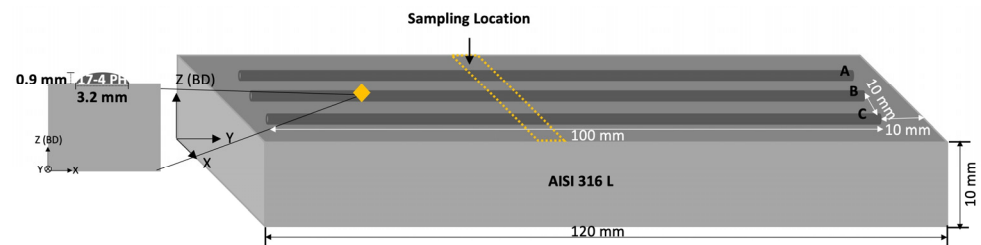


Figure 1. Scheme of the fabricated depositions: the yellow diamond indicates a transversal specimen drawn from one of the single tracks, whereas the yellow dotted line displays the sampling location.

The microstructure of the deposited tracks in the as-built condition was characterized using a Leica DMi8 A (Leica, Wetzlar, Germany) optical microscope (OM) according to the transversal sectioning in Figure 1. One transversal specimen for each deposition was carefully subjected to metallographic preparation following the ASTM E3 standard, involving grinding with SiC papers ranging from 120 to 1200 μm grit and subsequent polishing with diamond pastes ranging from 6 μm to 1 μm . After the metallographic preparation, chemical etching with Kalling's II (2g CuCl_2 , 40 mL HCl in 40–80 mL ethanol) for 10 s was performed.

Afterward, other transversal specimens were drawn from each single track and subjected to specifically settled PFHT routes. Three specimens, one from each single track, were then heat-treated according to five selected heat treatment routes, defined according to the outcomes of a preliminary investigation [8,39] and collected in Table 2. The first heat treatment (HT1) was similar to the conventional H900 treatment for 17-4 PH steels and consisted of: (i) a heating ramp of the specimens inside the furnace from room temperature to 1040 $^\circ\text{C}$ with a heating rate of 10 $^\circ\text{C}/\text{min}$; (ii) a solution treatment (SHT) performed at 1040 $^\circ\text{C}$ for 30 min, followed by water quenching; and (iii) final aging at 480 $^\circ\text{C}$ for 3 h. The

second heat treatment (HT2) differed from HT1 because no pre-heating was performed before SHT, i.e., the specimens were directly introduced into the oven at the settled SHT temperature of 1040 °C and held for 30 min. Conversely, the third heat treatment (HT3) was conducted providing for only direct aging carried out at 480 °C for 3 h, without a prior SHT step. In addition to these three heat treatment routes, long-time aging treatments were also established to explore the effect of aging time on the strengthening precipitation. The fourth heat treatment (HT4) was similar to HT1—involving a heating ramp of 10 °C/min, followed by SHT at 1040 °C for 30 min and subsequent water quenching—but with prolonging the aging duration up to 100 h. Lastly, the fifth heat treatment (HT5) was similar to HT3, but with providing for a direct aging duration of up to 100 h without SHT.

All the solubilization treatments were performed in a tubular Lenton LTF 12 oven (Lenton Furnaces & Ovens, Hope, Barnoldswick, UK), while the aging steps were carried out in a Remet E-79N muffle furnace (Remet di Franco Cicerchia & C. Sas, Casalecchio di Reno, Bologna). Throughout each heat treatment step, a K-type thermocouple was positioned inside the ovens and the temperature evolution was monitored and recorded using an OMEGA TC 08—Channel USB Thermocouple Data Acquisition Module (Omega, Norwalk, CT, USA) with Picolog 6 software (Pico Technology, Cambridgeshire, UK).

Table 2. Summary of the heat treatment routes applied in this work.

Heat Treatment Route	Heating Ramp	Solution Treatment	Quenching	Aging at 480 °C (h)
HT1	10 °C/min	1040 °C × 30 min	In water	3
HT2	NO	1040 °C × 30 min	In water	3
HT3	NO	NO	NO	3
HT4	10 °C/min	1040 °C × 30 min	In water	100
HT5	NO	NO	NO	100

As for the as-built specimens, the heat-treated ones were then subjected to the above-mentioned metallographic preparation and observed by using the same Leica DMi8 A optical microscope for a comprehensive analysis of their microstructural features.

To detect the phase compositions at the interface between the AISI 316L substrate and the 17-4 PH deposited tracks, a D8 Bruker (Bruker, MA, USA) X-ray diffractometer (XRD) with Cu K- α radiation collecting the pattern data from 20° to 110° (2 θ mode, 0.02° step size, and 1 s/step) was employed. Specifically, samples of about 8.9 × 8 × 2 mm³ in size (including the AISI 316 substrate and the 17-4 PH clads) were analyzed.

To investigate the presence of strengthening precipitates after the long-time aging treatments, one sample from each of the HT4 and HT5 specimens was prepared for observation using transmission electron microscopy (TEM). Thin specimens were fabricated from the peculiar shape of the track using the Crossbeam 340 (Carl Zeiss, Oberkochen, Germany) dual system focused ion beam—scanning electron microscope (FIB-SEM). The fabrication of the electron-transparent lamellas was performed in the upper part of the track, at a distance of about 120 μ m from the substrate and at an orientation for the lamella parallel to the steel substrate. The focused beam of Ga⁺ ions was accelerated at 30 keV for milling and at 5 keV for final polishing. The TEM analysis was carried out using an FEI Tecnai F20 (Thermo Fisher Instruments—formerly FEI, Hillsboro, OR, USA) high-resolution TEM (HRTEM) operating at 200 keV. Several imaging modes, including bright-field (BF) imaging, selected area electron diffraction (SAED), high-resolution electron microscopy (HREM), and scanning transmission imaging with high-angle annular dark-field (HAADF-STEM), were used. The average distance and the equivalent diameter of the detected strengthening particles were measured by the means of an image analysis.

Vickers microhardness measurements were conducted on specimens in the as-built and PFHT conditions, following the UNI EN ISO 6507-1:2018 standard [40]. At first, three linear microhardness profiles for each deposition were acquired by a Future-Tech FM1e Vickers microindenter (Future-Tech Corp., Kawasaki, Japan) under a 50 g_f load (HV0.05) with 15 s of loading time. In particular, the profiles were registered starting from the

substrate up to the tip of the depositions. The mean Vickers microhardness was then assessed at the center of each single track in the same conditions, as an average of ten random indentations.

3. Results and Discussion

3.1. Microstructural Analysis of the Specimens in the as-Built Condition

The representative OM micrographs of the microstructural features of the single tracks in the as-built condition, at the interface between the depositions and the AISI 316L substrate, are depicted in Figure 2. It can be seen that the single tracks exhibited a microstructure primarily composed of a lathy martensitic matrix, with a high amount of lathy δ -ferrite at the boundary between the steel plate and the depositions. The δ -ferrite was mainly localized at the interface because of the highest heat dissipation through the substrate. This is in agreement with other research [9,41] that proved that the microstructure of L-DED 17-4 PH steel is a result of the high heating and cooling rates experienced during the AM process (higher than those achieved during conventional ones), which prevent the formation of austenite [33,42,43]. Specifically, in the L-DED deposition of tracks on a metallic substrate, the highest cooling and solidification rates are found across the substrate/track interface, gradually decreasing with the distance from the substrate. Hence, in 17-4 PH single-track depositions, the high G·R ratios (G = thermal gradient ($^{\circ}\text{C}/\text{mm}$), R = growing speed (mm/s)) at the interface are expected to generate a fine martensitic matrix, but also a high amount of retained δ -ferrite

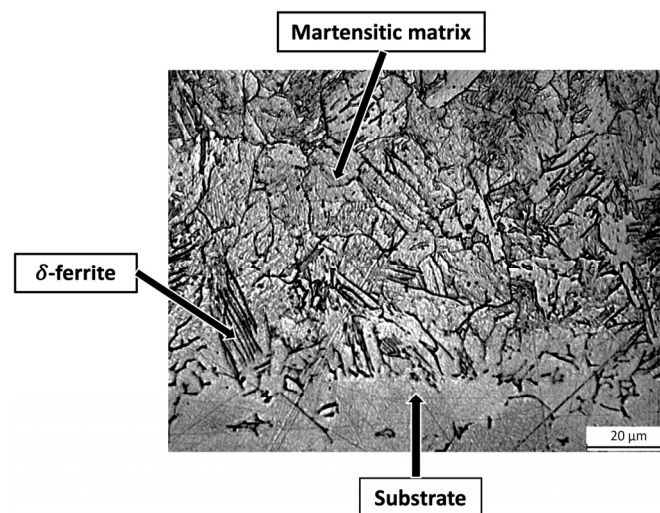


Figure 2. Representative OM micrograph of the microstructural features of the single tracks in the as-built condition, at the interface between the depositions and the AISI 316L substrate.

The X-ray diffraction pattern recorded on the single tracks in the as-built condition is shown in Figure 3. Considering the identified peaks, the presence of martensite (α') and austenite (γ) was confirmed; however, it should be noted that the austenite peaks can be attributed to the austenitic microstructure of the substrate due to the limited area of the deposited tracks. The δ -ferrite peaks were not identified because of the overlap with the crystallographic features of the α' -martensite, as already observed by other authors [43–45]. No other peaks related to the presence of strengthening precipitates were detected.

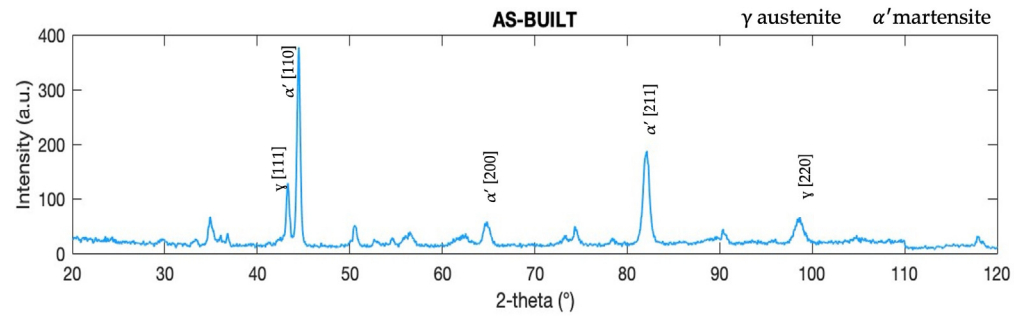


Figure 3. XRD pattern recorded on the single tracks in the as-built condition.

3.2. Microstructural Analysis of the Heat-Treated Specimens

In Figure 4, the representative microstructures of the deposited tracks after the different PFHTs are depicted. In the figure, the representative microstructures of the same tracks in the as-built condition are also reported as a reference (Figure 4a).

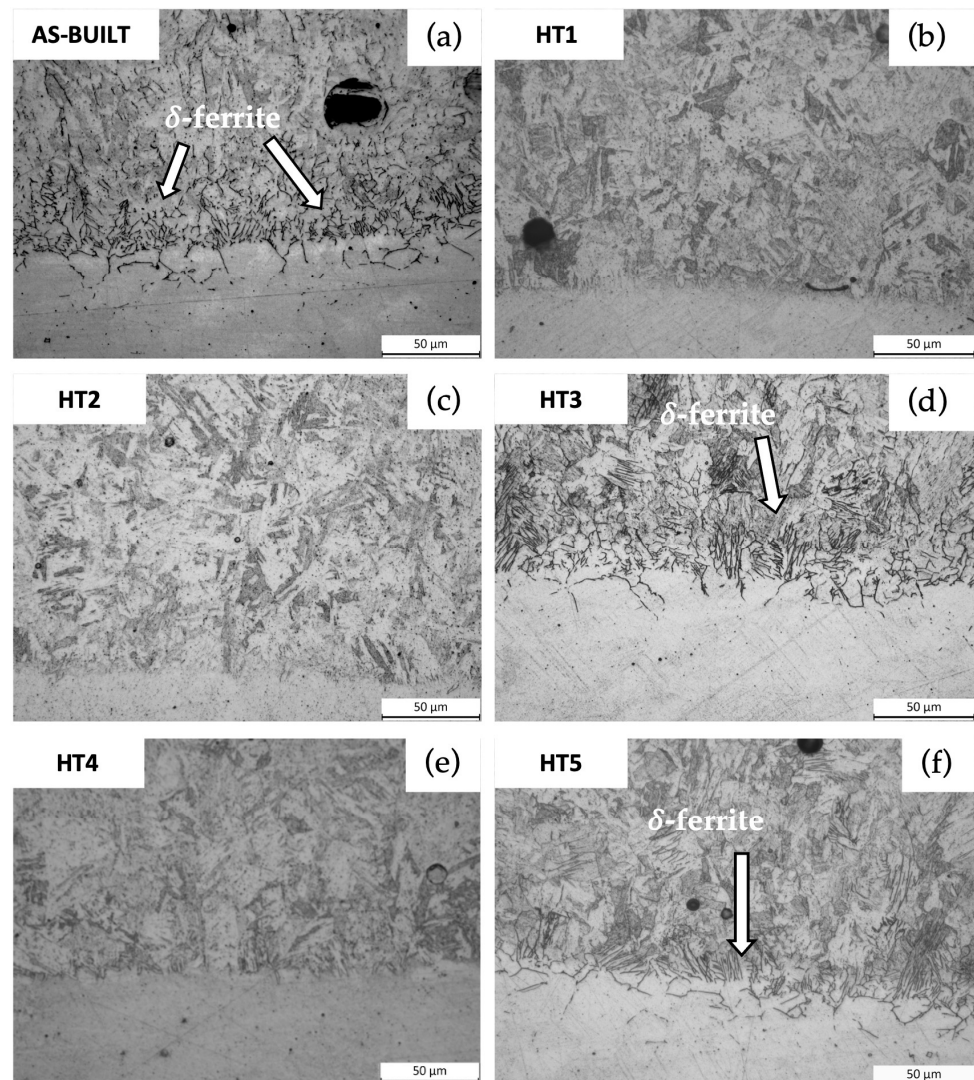


Figure 4. Representative OM micrographs of the microstructures of all specimens at the interface between the single tracks and the substrate: (a) as-built condition and after (b) HT1, (c) HT2, (d) HT3, (e) HT4, and (f) HT5 heat treatments.

As can be observed by comparing the micrographs of Figure 4a with those of Figure 4b,c, the SHT performed at 1040 °C for 30 min or for a shorter time (the HT1 and HT2 treatments, respectively) determined the dissolution of the lathy δ -ferrite. Similarly, no lathy δ -ferrite was detected in the specimens subjected to prolonged aging times of up to 100 h (HT4 treatment) (Figure 4e). It is worth noting that the efficacy of SHT in solubilizing the δ -ferrite phase in the austenitic matrix at a high temperature was previously reported in [46]. In addition, during SHT, most of the alloying elements are expected to dissolve in the matrix, generating a super-saturated solid solution after quenching at room temperature. In terms of the strengthening mechanism, it is well-known that, during the subsequent aging treatment, nanometric Cu-rich particles or Nb carbides precipitate in the martensitic matrix [47,48].

Conversely, in the HT3- and HT5-treated specimens (Figure 4d,f, respectively), which were subjected only to direct aging, the lathy δ -ferrite was still detectable, as in the as-built condition. Considering the high cooling rate induced by the L-DED process, a quasi-saturated condition for almost all alloying elements is expected, making the alloy prone to the precipitation of strengthening particles during aging. Nevertheless, as already mentioned, the detection of CRPs or Nb carbides remains challenging.

Figure 5 displays the X-ray diffraction spectra of the single tracks heat-treated according to the HT1, HT2, and HT3 routes, respectively. In all cases, peaks ascribed to the presence of α' -martensite and γ -austenite were identified. As already discussed in Section 3.1, previous studies [17,37,44] have confirmed that distinguishing δ -ferrite peaks from α' -martensite in the XRD patterns of 17-4 PH steel is difficult due to the low C concentration and their similar crystalline structures. Thus, irrespective of the heat treatment, α' -martensite peaks may encompass both phases, namely either δ -ferrite or α' -martensite. Moreover, it should be noted that a high-intensity [1 1 1] peak corresponding to the γ -austenite was evident. Some studies [25,49] have suggested that the presence of austenite in additively manufactured samples could be the result of prolonged exposure to medium to high temperatures during heat treatment, promoting the retention or the post-formation of the reverted austenite. In addition, AlMangour and Young proposed that long-time aging heat treatments in a non-protective atmosphere foster a high nitrogen presence, acting as an austenitic stabilizer and influencing the phase composition [38]. However, considering the narrow dimensions of the deposited tracks and the type of substrate adopted in the present study, the high-intensity [1 1 1] peak of γ -austenite may certainly be attributed to the austenitic matrix of the AISI 316L steel plate. No peaks related to the presence of nanometric Cu-rich particles or Nb carbides were detected in all the XRD spectra, due to their small size and quantity, together with their crystallographic parameters closely resembling those of the matrix [49,50]. In the literature, to enhance the study of strengthening particles, some authors have proposed performing aging treatments for times ranging from 2 to 200 h and up to 5000 h [36,51]. In these works, the use of transmission electron microscopy has been effective in detecting and identifying nanometric precipitates. Hence, two specimens subjected to long-time aging treatments, i.e., the HT4 and HT5 ones, were analyzed in depth by using TEM.

A TEM analysis was conducted on specimens that were HT4- and HT5-treated, focusing on the detection and identification of strengthening precipitates, specifically CRPs and Nb carbides, which can be expected after a long-time aging treatment. In Figure 6, two representative TEM micrographs of HT4 and HT5 specimens acquired in the BF imaging mode exhibit a polycrystalline microstructure. Both HT4 and HT5 feature a lathy martensite matrix. In the micrographs, the different contrast is mainly ascribed to the orientation of the crystal domains according to the direction of the electron beam of the TEM, while small-sized contrast details are an indication of defects within the matrix. The analysis of the electron diffraction pattern from selected areas (SAED) of the specimens confirmed the α' -martensite phase for both the HT4 and HT5 specimens.

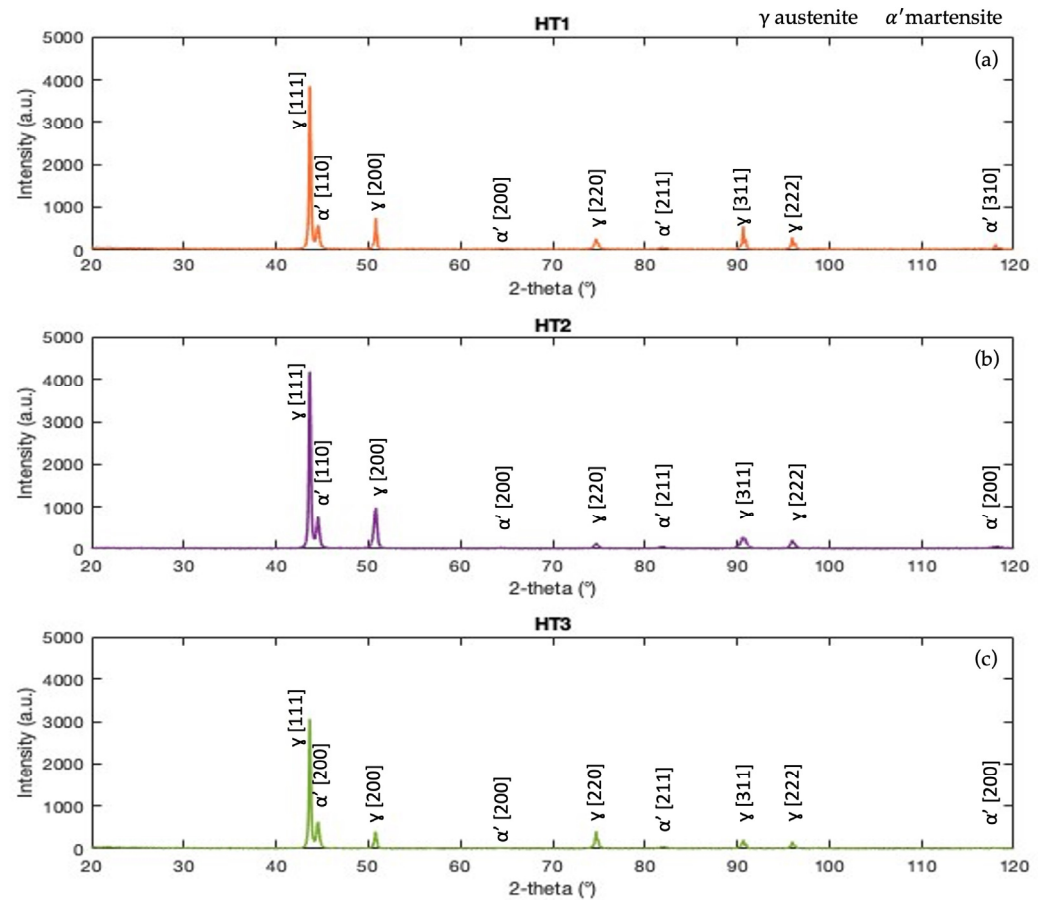


Figure 5. X-ray diffraction spectra of the single tracks heat-treated according to the (a) HT1, (b) HT2, and (c) HT3 routes.

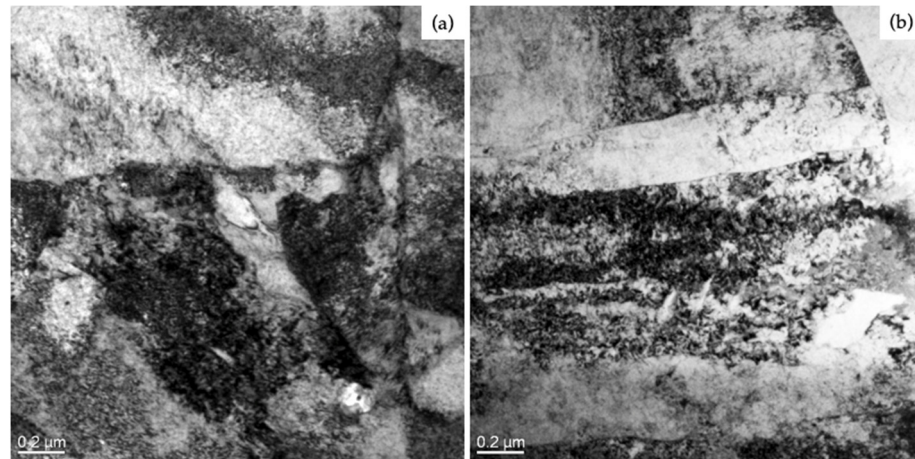


Figure 6. BF TEM micrographs of the microstructures of (a) HT4 and (b) HT5 specimens.

As previously mentioned, the SHT carried out at 1040 °C for 30 min promoted the dissolution of δ -ferrite and most of the alloying elements within the matrix. The subsequent aging treatment performed at 480 °C after rapid quenching was expected to promote the precipitation of nanometric Cu-rich particles and at least Nb carbides [48]. It is worth highlighting that, during the first 30–60 min of the aging treatment at 480 °C, the steel was expected to achieve its maximum hardness due to the precipitation of Cu clusters, which nucleate and grow coherently with the matrix until reaching the optimized size and density [48,52]. The TEM image shown in Figure 7a, obtained in the STEM-HAADF imaging mode to promote the compositional contrast, shows an example of a Nb carbide

particle. The white arrow in Figure 7a points to a low-contrast Nb carbide precipitate. Indeed, the decrease in contrast with respect to the surrounding iron matrix was ascribed to a lower value of both the average atomic number and density for the NbC precipitate [53]. In addition, the shape and size of the mentioned detail correspond to the NbC precipitates described in [36]. These carbides were dispersed in the thin lamella with an average distance of about 3.5 μm , and they measured about 92 nm in equivalent diameter. It is well-known that this type of carbide precipitates at 480 $^{\circ}\text{C}$ after 2 h of aging adjacent to Cu-rich nanometric particles [21]. In the HT4 specimen, an investigation performed on the grains at a high magnification and in the high-resolution imaging mode (Figure 7b) revealed the presence of small particles of a few nanometers in size. These features were identified as Cu-rich nanoparticles by the contrast fringes arising from the overlap between the particles and the martensitic lattice, as well as the analysis of the spatial frequencies in the high-resolution images. Figure 7c shows the Fast Fourier Transform (FFT) of the image reported in Figure 7b and features a regular lattice of spatial frequencies corresponding to the [0 0 1] zone-axis projection of the martensitic Fe; in addition, two extra spots marked by the white triangles highlight the presence of spatial frequencies not pertaining to the lattice of the Fe phase, and the lattice distance corresponding to these extra frequencies fits the [2 2 4] reflection for CuNi_3 at 0.101 nm [54]. Inverse FFT of the FFT pattern masked at the extra spots confirms that the moiré fringes in Figure 7b are the nanometric domains responsible for the extra frequencies.

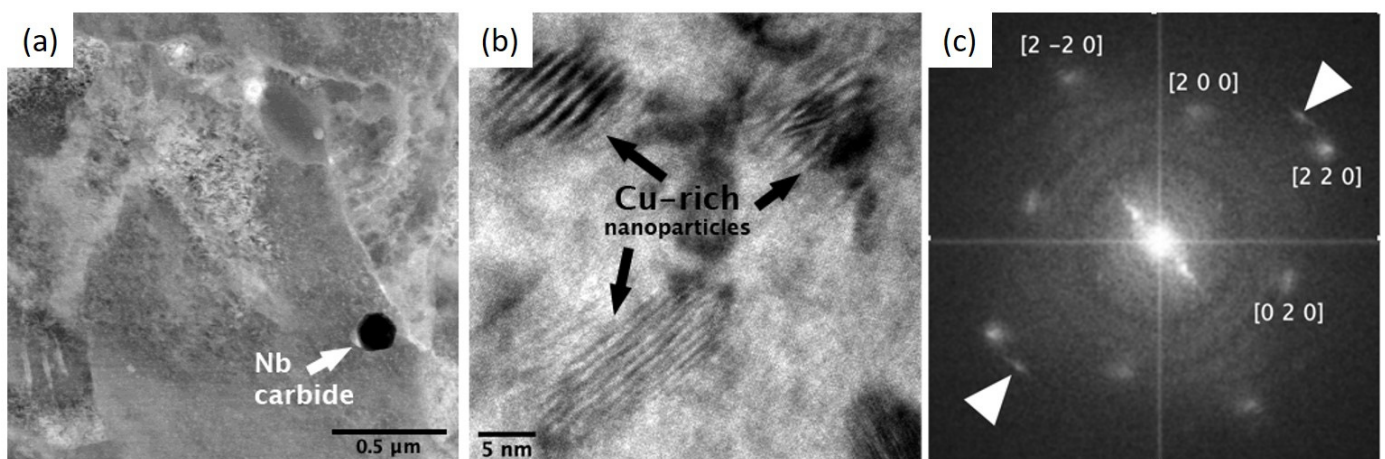


Figure 7. (a) STEM-HAADF images of HT4-treated specimen with a dark particle identified as Nb carbide (white arrow), (b) HRTEM view of the martensitic crystal domain with Cu-rich nanometric precipitates (black arrows), and (c) FFT of the image (b) with white triangles (c) pointing to extra spatial frequencies ascribed to Cu-rich precipitates.

The analysis performed on the HT5-treated specimen, which was subjected only to direct aging up to 100 h, revealed again the presence of only Nb carbides. The STEM-HAADF image reported in Figure 8 highlights the presence of NbC particles, similar to the ones previously observed in the HT4 specimen. Indeed, Figure 8 shows that the carbides were finer than the ones observed in the HT4 condition. These carbides were dispersed in the thin lamella with an average distance of about 2.7 μm , and they measured about 43 nm in equivalent diameter. This evidence agrees with other experimental findings, as reported in [21], with the authors affirming that the size of these carbides continued to increase until 120 h at 480 $^{\circ}\text{C}$. In [17], the authors confirmed that prolonged aging times at 480 $^{\circ}\text{C}$ induced the coarsening in size of the Nb carbides, even if this process was slower in case of direct aging. Other authors [55] suggested that Nb carbides and Cu-rich particles may appear over an extended period of up to around 9000 h, but at a lower aging temperature of 350 $^{\circ}\text{C}$.

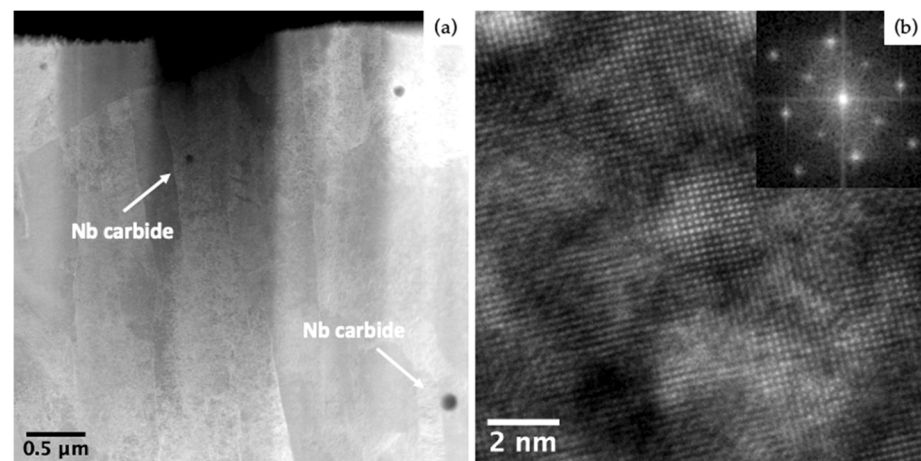


Figure 8. (a) STEM-HAADF images of HT5-treated specimen with the dark Nb carbides and (b) HRTEM view of the crystal domain (in the inset, the FFT of the TEM image with the spatial frequencies of the Fe lattice).

Conversely, considering the previous HT4-treated specimen, the HREM image and the corresponding FFT in the inset do not reveal the presence of nanometric domains within the Fe matrix which could possibly be attributed to Cu-based precipitates. In the HREM image, no evidence of moiré fringes arising from the superposition of crystal lattices was observed, and the analysis of the FFT of the HREM image did not reveal the presence of spatial frequencies belonging to a second phase other than the Fe matrix.

3.3. Hardness Behavior

In Figure 9, the mean microhardness profiles (HV0.05) measured from the substrate up to the tip of all heat-treated depositions are reported. In the graph, the mean microhardness profile of the specimens in the as-built condition is also shown and assumed as a reference. Concerning the specimens in the as-built condition, an average microhardness of about 392 HV0.05 was calculated within the deposited region. This value was mainly guaranteed by both the martensitic matrix and the δ -ferrite, whose presence was due to the high cooling rate induced by the L-DED process [56–58]. A sharp microhardness decrease was then measured at the interface between the single tracks and the substrate, because of the lower microhardness of the austenitic AISI 316L steel plate (about 295 HV0.05) with respect to that of the martensitic 17-4 PH deposited track (about 400 HV0.05 in the as-built condition).

Similar trends were found for the microhardness profiles measured in the heat-treated specimens, but with slight differences according to the adopted heat treatment routes. As for the specimens in the as-built condition, the profiles in Figure 9 show that the microhardness of all the heat-treated single tracks maintained a reasonable stability from the interface up to the tip of the depositions. In any case, the mean HV0.05 within the tracks was higher than that calculated in the as-built depositions; this evidence was probably due to the hardening effect provided by the fine precipitation of the Cu-rich nanometric particles or Nb carbides inside the deposited regions. At the interface between the track and the substrate, the HT1-, HT2-, and HT3-treated samples showed a steep drop in hardness of more than 100 HV0.05, until reaching mean values comparable to the microhardness of the steel plate. Local variations in HV0.05 inside the interface zone may be ascribed to the presence of the δ -ferrite.

In contrast, the HT4 and HT5 specimens displayed microhardness drops to average HV0.05 values slightly higher than those registered for the other heat treatments; due to the long-time aging treatment, a fine precipitation of $M_{23}C_6$ carbides may occur, increasing the hardness of the AISI 316L substrate [59,60].

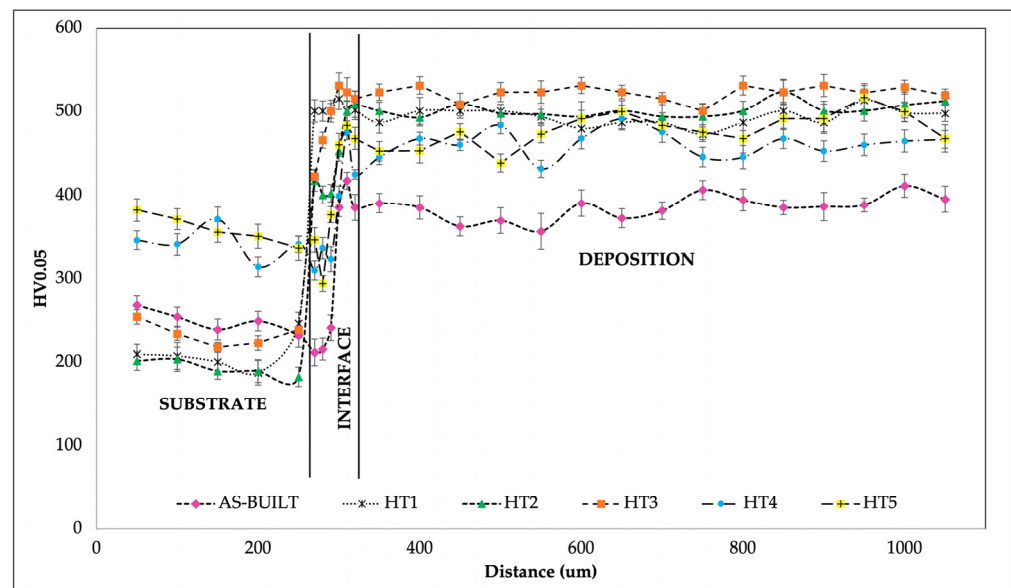


Figure 9. Mean Vickers microhardness profiles (HV0.05) measured from the substrate up to the tip of all the heat-treated depositions. In the graph, the mean microhardness profile of specimens in the as-built condition is also shown and assumed as a reference.

The mean Vickers microhardness \pm standard deviation of all the deposited regions is reported in Figure 10. The HT1, HT2, and HT3 routes determined a substantial increase (approximately in the range of 25–35%) in the mean microhardness of the heat-treated specimens as compared to that of the specimens in the as-built condition. In particular, direct aging performed for 3 h (corresponding to the HT3 treatment) provided the highest increase in HV0.05 (of about 35%), with an average microhardness of 523 HV0.05. These findings are in agreement with the literature, highlighting the effectiveness of direct aging in increasing the hardness of additively manufactured components [38]. Conversely, with an increase in the aging time (corresponding to the HT4 and HT5 treatments), a decrease in the mean microhardness was observed. As already mentioned in [52], with long-term aging at 480 °C, the CRPs start to coarsen, leading to an increase in their size and a decrease in their spatial density. However, it should be highlighted that, for longer aging times, small Nb carbides start to precipitate, thus contributing, to a minor extent, to the strengthening of the material. The HT4-treated specimens also showed a lower mean microhardness in comparison to that of the HT1-treated ones. As already discussed, long-time aging treatments (up to 100 h) performed after a complete SHT determined a coarsening effect in the Cu-rich strengthening particles. The presence of these precipitates was observed via the TEM analysis, confirming the occurrence of a coarsening effect. In addition, some Nb carbides were detected in the same transmission electron observations; these carbides were quite coarsened and rather distant from each other. The HT5-treated specimens, once again directly aged for 100 h, exhibited HV0.05 mean values higher than those obtained for the HT4-treated ones. In this case, no Cu-rich particles were detected via TEM, but smaller and closer Nb carbides, thus increasing the hardness of the alloy. This experimental finding is in agreement with the mean hardness values reported in Figure 10. At last, the mean microhardness of the HT5-treated specimens was similar to that of the HT1-treated depositions; this evidence further confirmed the efficacy of direct aging in enhancing the mechanical properties of a quasi-saturated metal matrix produced during the L-DED process [61]. Unfortunately, by comparing the mean HV0.05 resulting from the HT3 and HT5 heat treatments, prolonged aging times over 3 h seemed to have a negative effect on the mechanical properties of the single tracks. In fact, for a direct aging of 100 h (HT5), a microhardness decrease of about 9% was measured.

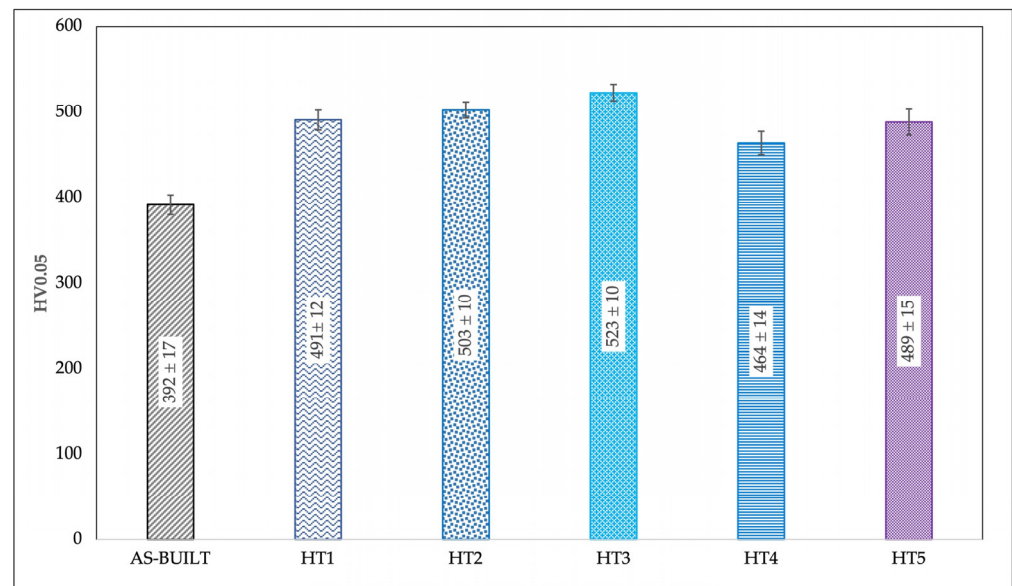


Figure 10. Mean Vickers microhardness values (HV0.05) \pm standard deviation of all deposited regions.

4. Conclusions

In this work, the effects on the microstructural and mechanical properties of L-DED 17-4 PH single-track depositions induced by specifically designed heat treatment routes, comprising a solution step followed by quenching and subsequent aging, were investigated and compared to those caused by long-term aging treatments or by direct aging.

Based on the results, the following conclusions can be drawn:

- In the as-built condition, the single tracks exhibited a microstructure composed of a lathy martensitic matrix with a high amount of lathy δ -ferrite, mainly located at the interface between the substrate and the depositions, with an average microhardness value of 392 ± 17 HV0.05.
- Five different PFHTs were settled and successfully applied to the 17-4 PH single tracks. The direct aging strategy demonstrated its efficacy in improving the mechanical properties of the depositions, with increments up to 35% as compared to the as-built condition. The best results were obtained after direct aging conducted for 3 h at 480 °C.
- XRD analyses confirmed that distinguishing δ -ferrite peaks from α' -martensite ones in the diffraction pattern of 17-4 PH steel is challenging due to the low C concentration and their similar crystalline structures. Irrespective of the heat treatment route, the α' -martensite peaks may encompass both phases, namely either δ -ferrite or α' -martensite.
- TEM analyses performed on specimens subjected to long-time aging of 100 h were able to reveal the presence of Cu-rich nanometric particles and Nb carbides. In the directly aged specimens, the precipitation mechanism was different from that observed in the specimens subjected to solution heat treatment before aging. In the directly aged specimens, the Nb carbides were finer and closer to each other than those in the specimens solubilized prior to aging. These findings further justified the measured microhardness values.

The understanding of the mechanism and sequence of precipitation of the strengthening particles in L-DED 17-4 PH depositions remains a challenge. A deeper investigation is ongoing, and the results will be compared to the ones discussed in this paper.

Author Contributions: Conceptualization, C.M. and M.M.; methodology, C.M., C.S., M.F. and M.M.; validation, C.M., C.S., M.F. and M.M.; investigation, C.M., M.F. and M.M.; resources, M.F. and M.M.; data curation, C.M. and M.M.; writing—original draft preparation, M.M. and C.M.; writing—review and editing, M.M., C.M., A.F., M.F. and C.S.; supervision, M.M.; project administration, M.M.; funding acquisition, M.M. and M.F. All authors have read and agreed to the published version of the manuscript.

Funding: This work was supported by the BiRex Corporation (Project AN-MEC—L'Additive Manufacturing nella filiera produttiva dell'industria meccanica: dallo sviluppo del processo alla definizione del business model per la produzione di nuovi componenti", CUP C41J20000030008).

Institutional Review Board Statement: Not applicable.

Informed Consent Statement: Not applicable.

Data Availability Statement: The authors confirm that the processed data supporting the findings of this study are available within the article. The raw data not explicitly reported in the article are available on request.

Acknowledgments: The authors wish to acknowledge Alessandro Fortunato for providing the samples analyzed in the present research. The authors also acknowledge Gabriele Bertocchi for his support in the XRD analyses.

Conflicts of Interest: The authors declare that this study received funding from BiRex Corporation. The funder was not involved in the study design, collection, analysis, interpretation of data, the writing of this article or the decision to submit it for publication.

References

1. ASTM A693-22; ASTM International Standard Specification for Precipitation-Hardening Stainless and Heat-Resisting Steel Plate, Sheet, and Strip. ASTM: West Conshohocken, PA, USA, 2022.
2. Murthy, A.S. Role of Alloy Additions on Strengthening in 17-4 PH Stainless Steel. Ph.D. Thesis, Missouri University of Science and Technology, Rolla, MO, USA, 2012.
3. Steponavičiute, A.; Selskiene, A.; Stravinskas, K.; Borodinas, S.; Mordas, G. 17-4 PH Stainless-Steel as a Material for High Resolution Laser Metal Deposition. *Mater. Today Proc.* **2021**, *52*, 2268–2272. [CrossRef]
4. ISO/ASTM 52900; Additive Manufacturing—General Principles. ASTM International Standard: West Conshohocken, PA, USA, 2015; pp. 1–28.
5. ASTM F3187-16; Standard Guide for Directed Energy Deposition of Metals. ASTM International: West Conshohocken, PA, USA, 2016; pp. 1–22.
6. ASTM F2792-12; ASTM Standard Terminology for Additive Manufacturing Technologies F2792. ASTM: West Conshohocken, PA, USA, 2012.
7. Mathoho, I.; Akinlabi, E.T.; Arthur, N.; Tlotleng, M. Impact of DED Process Parameters on the Metallurgical Characteristics of 17-4 PH SS Deposited Using DED. *CIRP J. Manuf. Sci. Technol.* **2020**, *31*, 450–458. [CrossRef]
8. Morales, C.; Merlin, M.; Fortini, A.; Fortunato, A. Direct Energy Depositions of a 17-4 PH Stainless Steel: Geometrical and Microstructural Characterizations. *Coatings* **2023**, *13*, 636. [CrossRef]
9. Badi, L. Effect of Process Parameters on the Quality of 17-4 PH Samples Produced by Directed Energy Deposition. Master's Thesis, Politecnico di Torino, Turin, Italy, 2021.
10. Pan, L.; Kwok, C.T.; Niu, B.; Huang, X.; Cao, Y.; Zou, X.; Yi, J. Enhancement in Hardness and Corrosion Resistance of Directed Energy Deposited 17-4 PH Martensitic Stainless Steel via Heat Treatment. *J. Mater. Res. Technol.* **2023**, *23*, 1296–1311. [CrossRef]
11. Tacq, Jeroen. L-PBF and Heat Treatment of 17-4PH Steel. 2021. Available online: https://static.fcomedia.be/user/11/images/inside_metal_am_3d_printing_with_steel.pdf (accessed on 25 May 2022).
12. Hu, Z.; Zhu, H.; Zhang, H.; Zeng, X. Experimental Investigation on Selective Laser Melting of 17-4PH Stainless Steel. *Opt. Laser Technol.* **2017**, *87*, 17–25. [CrossRef]
13. Bayode, A.; Pityana, S.; Akinlabi, E.T.; Shongwe, M.B. Effect of Scanning Speed on Laser Deposited 17-4PH Stainless Steel. In Proceedings of the 2017 8th International Conference on Mechanical and Intelligent Manufacturing Technologies, ICMIMT 2017, Cape Town, South Africa, 3–6 February 2017; pp. 1–5. [CrossRef]
14. Gu, H.; Gong, H.; Pal, D.; Rafi, K.; Starr, T.; Stucker, B. Influences of Energy Density on Porosity and Microstructure of Selective Laser Melted 17-4PH Stainless Steel. In Proceedings of the 24th International SFF Symposium—An Additive Manufacturing Conference, SFF 2013, Austin, TX, USA, 12–14 August 2013; pp. 474–489.
15. Auguste, P.; Mauduit, A.; Fouquet, L.; Pillot, S. Study on 17-4 PH Stainless Steel Produced by Selective Laser Melting. *UPB Sci. Bull. Ser. B Chem. Mater. Sci.* **2018**, *80*, 197–210.
16. Pham, L.; Lu, G.; Tran, P. Influences of Printing Pattern on Mechanical Performance of Three-Dimensional-Printed Fiber-Reinforced Concrete. *3D Print. Addit. Manuf.* **2022**, *9*, 46–63. [CrossRef]

17. Zhou, T.; Zheng, T.; Yildiz, A.B.; Spartacus, G.; Rolinska, M.; Cubitt, R.; Hedström, P. Microstructure Control during Deposition and Post-Treatment to Optimize Mechanical Properties of Wire-Arc Additively Manufactured 17-4 PH Stainless Steel. *Addit. Manuf.* **2022**, *58*, 103047. [[CrossRef](#)]
18. Lashgari, H.R.; Kong, C.; Adabifiroozjaei, E.; Li, S. Microstructure, Post Thermal Treatment Response, and Tribological Properties of 3D Printed 17-4 PH Stainless Steel. *Wear* **2020**, *456–457*, 203367. [[CrossRef](#)]
19. Cheruvathur, S.; Lass, E.A.; Campbell, C.E. Additive Manufacturing of 17-4 PH Stainless Steel: Post-Processing Heat Treatment to Achieve Uniform Reproducible Microstructure. *Miner. Met. Mater. Soc. ASM Int.* **2016**, *68*, 930–942. [[CrossRef](#)]
20. Stornelli, G.; Gaggia, D.; Rallini, M.; Di Schino, A. Heat Treatment Effect on Maraging Steel Manufactured by Laser Powder Bed Fusion Technology: Microstructure and Mechanical Properties. *Acta Metall. Slovaca* **2021**, *27*, 122–126. [[CrossRef](#)]
21. Yeli, G.; Auger, M.A.; Wilford, K.; Smith, G.D.W.; Bagot, P.A.J.; Moody, M.P. Sequential Nucleation of Phases in a 17-4PH Steel: Microstructural Characterisation and Mechanical Properties. *Acta Mater.* **2017**, *125*, 38–49. [[CrossRef](#)]
22. Mirzadeh, H.; Najafizadeh, A. Aging Kinetics of 17-4 PH Stainless Steel. *Mater. Chem. Phys.* **2009**, *116*, 119–124. [[CrossRef](#)]
23. ASM International Heat Treating. In *ASM Handbook*; ASM International: Novelty, OH, USA, 1991; Volume 4, pp. 1–2173.
24. Stoudt, M.R.; Ricker, R.E.; Lass, E.A.; Levine, L.E. Influence of Postbuild Microstructure on the Electrochemical Behavior of Additively Manufactured 17-4 PH Stainless Steel. *JOM* **2017**, *69*, 506–515. [[CrossRef](#)]
25. LeBrun, T.; Nakamoto, T.; Horikawa, K.; Kobayashi, H. Effect of Retained Austenite on Subsequent Thermal Processing and Resultant Mechanical Properties of Selective Laser Melted 17-4 PH Stainless Steel. *Mater. Des.* **2015**, *81*, 44–53. [[CrossRef](#)]
26. Hsu, T.-H.; Chang, Y.-J.; Huang, C.-Y.; Yen, H.-W.; Chen, C.-P.; Jen, K.-K.; Yeh, A.-C. Microstructure and Property of a Selective Laser Melting Process Induced Oxide Dispersion Strengthened 17-4 PH Stainless Steel. *J. Alloys Compd.* **2019**, *803*, 30–41. [[CrossRef](#)]
27. Meredith, S.D.; Zuback, J.S.; Keist, J.S.; Palmer, T.A. Impact of Composition on the Heat Treatment Response of Additively Manufactured 17-4 PH Grade Stainless Steel. *Mater. Sci. Eng. A* **2018**, *738*, 44–56. [[CrossRef](#)]
28. Mahmoudi, M.; Elwany, A.; Yadollahi, A.; Thompson, S.M.; Bian, L.; Shamsaei, N. Mechanical Properties and Microstructural Characterization of Selective Laser Melted 17-4 PH Stainless Steel. *Rapid Prototyp. J.* **2017**, *23*, 280–294. [[CrossRef](#)]
29. Pasebani, S.; Ghayoor, M.; Badwe, S.; Irrinki, H.; Atre, S. V Effects of Atomizing Media and Post Processing on Mechanical Properties of 17-4 PH Stainless Steel Manufactured via Selective Laser Melting. *Addit. Manuf.* **2018**, *22*, 127–137. [[CrossRef](#)]
30. AlMangour, B.; Grzesiak, D.; Yang, J.M. Scanning Strategies for Texture and Anisotropy Tailoring during Selective Laser Melting of TiC/316L Stainless Steel Nanocomposites. *J. Alloys Compd.* **2017**, *728*, 424–435. [[CrossRef](#)]
31. Murr, L.E.; Martinez, E.; Hernandez, J.; Collins, S.; Amato, K.N.; Gaytan, S.M.; Shindo, P.W. Microstructures and Properties of 17-4 PH Stainless Steel Fabricated by Selective Laser Melting. *J. Mater. Res. Technol.* **2012**, *1*, 167–177. [[CrossRef](#)]
32. Rafi, H.K.; Pal, D.; Patil, N.; Starr, T.L.; Stucker, B.E. Microstructure and Mechanical Behavior of 17-4 Precipitation Hardenable Steel Processed by Selective Laser Melting. *J. Mater. Eng. Perform.* **2014**, *23*, 4421–4428. [[CrossRef](#)]
33. Ziewiec, A.; Zielińska-Lipiec, A.; Kowalska, J.; Ziewiec, K. Microstructure Characterization of Welds in X5CrNiCuNb16-4 Steel in Overaged Condition. *Adv. Mater. Sci.* **2019**, *19*, 57–69. [[CrossRef](#)]
34. Sowa, R.; Kowal, A.; Roga, E.; Arabasz, S.; Dziedzic, A.; Dul, I.; Parlinska-Wojtan, M. Influence of Double Solution Treatment on Hardness in 17-4 PH Steel. *Zast. Mater.* **2015**, *56*, 261–268. [[CrossRef](#)]
35. Viswanathan, U.K.; Banerjee, S.; Krishnan, R. Effects of Aging on the Microstructure of 17-4 PH Stainless Steel. *Mater. Sci. Eng. A* **1988**, *104*, 181–189. [[CrossRef](#)]
36. Murayama, M.; Katayama, Y.; Hono, K. Microstructural Evolution in a 17-4 PH Stainless Steel after Aging at 400 C. *Metall. Mater. Trans. A* **1999**, *30*, 345–353. [[CrossRef](#)]
37. Sun, Y.; Hebert, R.J.; Aindow, M. Effect of Heat Treatments on Microstructural Evolution of Additively Manufactured and Wrought 17-4PH Stainless Steel. *Mater. Des.* **2018**, *156*, 429–440. [[CrossRef](#)]
38. AlMangour, B.; Yang, J.-M. Understanding the Deformation Behavior of 17-4 Precipitate Hardenable Stainless Steel Produced by Direct Metal Laser Sintering Using Micropillar Compression and TEM. *Int. J. Adv. Manuf. Technol.* **2017**, *90*, 119–126. [[CrossRef](#)]
39. Morales, C.; Merlin, M.; Debdoubi, F.; Fortini, A.; Ferrucci, P. *La Metallurgia Italiana*; SpiderWeb: Ferrara, Italy, 2023; pp. 42–47.
40. *UNI EN ISO 6507-1:2018*; Metallic Materials—Vickers Hardness Test—Part 1: Test Method. ISO: Geneva, Switzerland, 2018.
41. Li, J.; Cheng, L.; Zhang, P.; Wang, L.; Li, H. Effect of Delta Ferrites on the Anisotropy of Impact Toughness in Martensitic Heat-Resistant Steel. *J. Mater. Res. Technol.* **2019**, *8*, 1781–1788. [[CrossRef](#)]
42. Bahrami Balajaddeh, M.; Naffakh-Moosavy, H. Pulsed Nd:YAG Laser Welding of 17-4 PH Stainless Steel: Microstructure, Mechanical Properties, and Weldability Investigation. *Opt. Laser Technol.* **2019**, *119*, 105651. [[CrossRef](#)]
43. Garcia-Cabezón, C.; Castro-Sastre, M.A.; Fernandez-Abia, A.I.; Rodriguez-Mendez, M.L.; Martin-Pedrosa, F. Microstructure–Hardness–Corrosion Performance of 17-4 Precipitation Hardening Stainless Steels Processed by Selective Laser Melting in Comparison with Commercial Alloy. *Met. Mater. Int.* **2022**, *28*, 2652–2667. [[CrossRef](#)]
44. Nezhadfar, P.D.; Burford, E.; Anderson-Wedge, K.; Zhang, B.; Shao, S.; Daniewicz, S.R.; Shamsaei, N. Fatigue Crack Growth Behavior of Additively Manufactured 17-4 PH Stainless Steel: Effects of Build Orientation and Microstructure. *Int. J. Fatigue* **2019**, *123*, 168–179. [[CrossRef](#)]
45. Feng, Z. The Lattice Parameter of Gamma Iron and Iron-Chromium Alloys. Master’s Thesis, Case Western Reserve University, Cleveland, OH, USA, 2015.

46. Li, K.; Sridar, S.; Tan, S.; Xiong, W. Effect of Homogenization on Precipitation Behavior and Strengthening of 17-4PH Stainless Steel Fabricated Using Laser Powder Bed Fusion. *arXiv* **2021**, arXiv:2112.06289.
47. Ščetinec, A.; Klobčar, D.; Nagode, A.; Vuherer, T.; Bračun, D.; Trdan, U. Optimisation of Precipitation Hardening for 15-5 PH Martensitic Stainless Steel Produced by Wire Arc Directed Energy Deposition. *Sci. Technol. Weld. Join.* **2023**, *28*, 558–568. [[CrossRef](#)]
48. Rowolt, C.; Milkereit, B.; Springer, A.; Kreyenschulte, C.; Kessler, O. Dissolution and Precipitation of Copper-Rich Phases during Heating and Cooling of Precipitation-Hardening Steel X5CrNiCuNb16-4 (17-4 PH). *J. Mater. Sci.* **2020**, *55*, 13244–13257. [[CrossRef](#)]
49. Villa, M.; Grumsen, F.B.; Niessen, F.; Dahmen, T.; Cao, L.; Reich, M.; Kessler, O.; Huang, X.; Somers, M.A.J. Aging 17-4 PH Martensitic Stainless Steel Prior to Hardening: Effects on Martensitic Transformation, Microstructure and Properties. *Materialia* **2023**, *32*, 101882. [[CrossRef](#)]
50. Wang, Z.; Li, H.; Shen, Q.; Liu, W.; Wang, Z. Nano-Precipitates Evolution and Their Effects on Mechanical Properties of 17-4 Precipitation-Hardening Stainless Steel. *Acta Mater.* **2018**, *156*, 158–171. [[CrossRef](#)]
51. Wang, J.; Zou, H.; Li, C.; Qiu, S.; Shen, B. The Spinodal Decomposition in 17-4PH Stainless Steel Subjected to Long-Term Aging at 350 °C. *Mater. Charact.* **2008**, *59*, 587–591. [[CrossRef](#)]
52. Yan, S.; Wang, Z.; Li, T.; Chen, Z.; Du, X.; Liu, Y.; Chen, D.; Sun, K.; Liu, R.; Bai, B.; et al. In Situ Characterization of 17-4PH Stainless Steel by Small-Angle Neutron Scattering. *Materials* **2023**, *16*, 5583. [[CrossRef](#)]
53. Cuppari, M.G.d.V.; Santos, S.F. Physical Properties of the NbC Carbide. *Metals* **2016**, *6*, 250. [[CrossRef](#)]
54. Materials Explorer. Available online: <https://next-gen.materialsproject.org/materials/mp-1184054?formula=CuNi3> (accessed on 29 December 2023).
55. Wang, J.; Zou, H.; Li, C.; Peng, Y.; Qiu, S.; Shen, B. The Microstructure Evolution of Type 17-4PH Stainless Steel during Long-Term Aging at 350 °C. *Nucl. Eng. Des.* **2006**, *236*, 2531–2536. [[CrossRef](#)]
56. Sun, Y.; Hebert, R.J.; Aindow, M. Effect of Laser Scan Length on the Microstructure of Additively Manufactured 17-4PH Stainless Steel Thin-Walled Parts. *Addit. Manuf.* **2020**, *35*, 101302. [[CrossRef](#)]
57. Haines, M.P.; Moyle, M.S.; Rielli, V.V.; Luzin, V.; Haghdadadi, N.; Primig, S. Experimental and Computational Analysis of Site-Specific Formation of Phases in Laser Powder Bed Fusion 17-4 Precipitate Hardened Stainless Steel. *Addit. Manuf.* **2023**, *73*, 103686. [[CrossRef](#)]
58. Alkan, G.; Chae, D.; Kim, S.J. Effect of δ Ferrite on Impact Property of Hot-Rolled 12Cr-Ni Steel. *Mater. Sci. Eng. A* **2013**, *585*, 39–46. [[CrossRef](#)]
59. Benoit, M.J.; Tabaie, S.; Waqar, T.; Ganton, T.; Amirkhiz, B.S.; Hadadzadeh, A.; Nasiri, A. Effects of Additive Manufacturing Processes and Isothermal Aging on the Microstructure and Properties of 13-8 Mo Precipitation Hardening Martensitic Stainless Steel. *Addit. Manuf.* **2023**, *72*, 103615. [[CrossRef](#)]
60. Fang, K.; Luo, K.; Wang, L. Effect of Microstructure on Mechanical Properties of 316 LN Austenitic Stainless Steel. *Coatings* **2022**, *12*, 1461. [[CrossRef](#)]
61. Chae, H.; Luo, M.Y.; Huang, E.W.; Shin, E.; Do, C.; Hong, S.K.; Woo, W.; Lee, S.Y. Unearthing Principal Strengthening Factors Tuning the Additive Manufactured 15-5 PH Stainless Steel. *Mater. Charact.* **2022**, *184*, 111645. [[CrossRef](#)]

Disclaimer/Publisher’s Note: The statements, opinions and data contained in all publications are solely those of the individual author(s) and contributor(s) and not of MDPI and/or the editor(s). MDPI and/or the editor(s) disclaim responsibility for any injury to people or property resulting from any ideas, methods, instructions or products referred to in the content.